The Astrophysical Journal, 723:1512–1522, 2010 November 10 doi:10.1088/0004-637X/723/2/1512

EFFECT OF HIGH-ENERGY RESONANCES ON THE $^{18}O(p,\alpha)^{15}N$ REACTION RATE AT AGB AND POST-AGB RELEVANT TEMPERATURES

M. La Cognata[1], C. Spitaleri[1], and A. M. Mukhamedzhanov[2]
[1] INFN-Laboratori Nazionali del Sud and University of Catania, I-95123 Catania, Italy; lacognata@lns.infn.it
[2] Cyclotron Institute-Texas A&M University, College Station, TX, USA
Received 2010 June 26; accepted 2010 September 8; published 2010 October 25

ABSTRACT

The $^{18}O(p,\alpha)^{15}N$ reaction is of great importance in several astrophysical scenarios, as it influences the production of key isotopes such as ^{19}F, ^{18}O, and ^{15}N. Fluorine is synthesized in the intershell region of asymptotic giant branch (AGB) stars, together with *s*-elements, by α radiative capture on ^{15}N, which in turn is produced in the ^{18}O proton-induced destruction. Peculiar ^{18}O abundances are observed in R-Coronae Borealis stars, having $^{16}O/^{18}O \lesssim 1$, hundreds of times smaller than the galactic value. Finally, there is no definite explanation of the $^{14}N/^{15}N$ ratio in pre-solar grains formed in the outer layers of AGB stars. Again, such an isotopic ratio is influenced by the $^{18}O(p,\alpha)^{15}N$ reaction. In this work, a high accuracy $^{18}O(p,\alpha)^{15}N$ reaction rate is proposed, based on the simultaneous fit of direct measurements and of the results of a new Trojan Horse experiment. Indeed, current determinations are uncertain because of the poor knowledge of the resonance parameters of key levels of ^{19}F. In particular, we have focused on the study of the broad 660 keV $1/2^+$ resonance corresponding to the 8.65 MeV level of ^{19}F. Since $\Gamma \sim 100$–300 keV, it determines the low-energy tail of the resonant contribution to the cross section and dominates the cross section at higher energies. Here, we provide a reaction rate that is a factor of two larger above $T \sim 0.5\,10^9$ K based on our new improved determination of its resonance parameters, which could strongly influence present-day astrophysical model predictions.

Key words: nuclear reactions, nucleosynthesis, abundances – stars: abundances – stars: AGB and post-AGB

Online-only material: color figures

1. INTRODUCTION

In recent years, both models and observations have reached a high degree of accuracy in several astrophysical environments. This has allowed researchers to single out key problems or critical points deserving closer attention. The $^{18}O(p,\alpha)^{15}N$ reaction has been proven to play a key role as it influences the production of isotopes such as ^{19}F, ^{18}O, and ^{15}N that can be used to probe several astrophysical scenarios and test the current accepted models. In particular, ^{19}F has been the subject of extensive investigations, regarding both its spectroscopic determination in the cold outermost layers of asymptotic giant branch (AGB) stars (Abia et al. 2010, 2009a, 2009b) and its nucleosynthesis in the intershell region of AGB stars (Lugaro et al. 2004). These studies have been triggered by the possibility of using fluorine abundance to constrain AGB models as it is sensitive to the efficiency of the dredge-up and to the physical conditions in the deep layers of AGB stars (Lugaro et al. 2004).

Peculiar ^{18}O and ^{19}F abundances are observed in post-AGB stars, in particular in the so-called R-Coronae Borealis stars, having $^{16}O/^{18}O \lesssim 1$, hundreds of times smaller than the galactic value (the solar ratio is 500), and fluorine enhancements by factors of 800–8000 with respect to the supposed initial abundances (Clayton et al. 2007; Pandey et al. 2008). The recent work by Clayton et al. (2007) has pointed out that a quantitative account of such abundances can be provided only in the framework of the double degenerate scenario. In fact, Clayton et al. (2007) have also shown that, if the $^{18}O(p,\alpha)^{15}N(p,\alpha)^{12}C$ chain is activated, the $^{16}O/^{18}O$ and the C/N ratios reach observed values, thus reversing the effect of excessive He burning, while fluorine is produced by *p*-radiative captures on ^{18}O. Therefore, a revised $^{18}O(p,\alpha)^{15}N$ reaction rate at temperatures higher than those in AGB stars might provide a clue to better understanding these rare systems.

Precious information about nucleosynthesis inside AGB stars is provided by the abundance ratios of some CNO and aluminum isotopes, such as ^{18}O, ^{17}O, ^{15}N, ^{13}C, and ^{26}Al, to the corresponding most abundant ones, namely ^{16}O, ^{14}N, ^{12}C, and ^{27}Al (Nollett et al. 2003; Busso et al. 2010), which are very sensitive to the nucleosynthesis and the mixing mechanisms taking place inside these stars. These isotopic ratios are determined with good accuracy from the analysis of meteorite grains (Zinner 2005). Though current AGB models can explain several features of the measured isotopic ratio patterns, several questions are still open that nuclear physics might help to answer without introducing additional hypotheses on mixing processes. In particular, a revised $^{18}O(p,\alpha)^{15}N$ reaction rate might shed light on the $^{14}N/^{15}N$ isotopic ratio, which turns out to be even smaller than the solar one.

It is worth stressing that, following the above considerations, an accurate knowledge of the $^{18}O(p,\alpha)^{15}N$ reaction rate is required over a wide temperature range, $T_9 = 0.007$–0.5 ($T_9 = T/10^9$ K). Therefore, an accurate knowledge of its cross section in the 0–1 MeV energy range is also required.

2. PREVIOUS MEASUREMENTS

About 10 resonances contribute to the $^{18}O(p,\alpha)^{15}N$ reaction cross section below 1 MeV (Lorentz-Wirzba et al. 1979; Angulo et al. 1999). In particular, the narrow $E_R = 20$ keV $5/2^+$ resonance (corresponding to the $E_x = 8.014$ MeV state of ^{19}F) is especially important at $T_9 \lesssim 0.02$ (La Cognata et al. 2009a, 2010), the narrow 145 keV $1/2^+$ resonance ($E_x = 8.138$ MeV) dominates the reaction rate for $0.05 \lesssim T_9 \lesssim 1$ (Lorentz-Wirzba et al. 1979), while the broad 799 keV $1/2^+$ resonance

Table 1
Level Parameters for 660 keV Resonance

E_R (keV)	Γ_p (keV)	Γ_α (keV)	Γ_{tot} (keV)	References
~658	~7	~317	~324	Lorentz-Wirzba et al. (1979)
616	5	150	155	Mak et al. (1978)
644	4.7	90	94.7	Yagi (1962)
656	...	...	~300	Tilley et al. (1995)
656 ± 30	5.6 ± 1.0	200 ± 110	206 ± 110	Iliadis et al. (2010)
590 ± 20	...	...	208 ± 26	La Cognata et al. (2008a)

Notes. Each parameter is given in the center-of-mass system. The parameters taken from Lorentz-Wirzba et al. (1979) and Mak et al. (1978) are obtained from the *R*-matrix parameterizations of the measured $^{18}O(p,\alpha)^{15}N$ reaction cross sections. In the same way, Yagi (1962) extracted the resonance parameters from the *R*-matrix fitting of the $^{18}O + p$ elastic scattering. Tilley et al. (1995) and Iliadis et al. (2010) are reviews of the existing data. Finally, La Cognata et al. (2008a) is a recent indirect preliminary measurement by means of the THM.

($E_x = 8.793$ MeV) has a significant contribution at high temperatures (Angulo et al. 1999). These levels have been the subject of direct and indirect studies (compare Champagne & Pitt 1986; Wiescher & Kettner 1982; La Cognata et al. 2009a, 2010; Wiescher et al. 1980, Mak et al. 1978; Lorentz-Wirzba et al. 1979; Wiescher et al. 1980, and Lorentz-Wirzba et al. 1979; Yagi 1962; Wiescher et al. 1980; Christensen et al. 1990 for the 20, 145, and 799 keV resonances, respectively). Thus, the contribution to the reaction rate from such resonances is presently well established.

Particular attention has to be devoted to the broad $1/2^+$ resonance at about 660 keV. Our present knowledge allows us to state that it is comparatively broad, Γ_{tot} ranging from 100 to 300 keV according to the different measurements (Yagi 1962; Lorentz-Wirzba et al. 1979; Mak et al. 1978). As a consequence, such a broad resonance at 660 keV gives strong contributions at both low and high temperatures (Angulo et al. 1999) and its accurate determination is crucial to pin down both the reaction rate and its uncertainty. Furthermore, all the measurements are in agreement regarding the proton width, $\Gamma_p \sim 5$ keV, but not for the α-particle width ($\Gamma_\alpha = 317$, keV Lorentz-Wirzba et al. 1979; 150 keV, Mak et al. 1978; or 90 keV, Yagi 1962). The resonance energy E_R, the proton and α widths Γ_p and Γ_α, and the total width are summarized in Table 1. To account for the large discrepancy in the NACRE compilation (Angulo et al. 1999) the contribution of the 660 keV resonance to the reaction rate has been evaluated by averaging the rates resulting from the numerical integration of the cross sections obtained from the two sets of widths available, namely from Yagi (1962) and Lorentz-Wirzba et al. (1979). To underscore the importance of the 8.65 MeV ^{19}F state, we note that its updated contribution accounted for the differences between the adopted NACRE rate (Angulo et al. 1999) and the CF88 one (Coughlan & Fowler 1988) at high temperatures ($T9 > 0.45$). In a similar approach, Iliadis et al. (2010) adopted a value of $\Gamma_\alpha = 200 \pm 110$ keV, which is an average of the existing widths, in the reaction rate calculations. Finally, a preliminary Trojan Horse Method (THM) measurement of the 660 keV resonance has been performed, aiming at extracting the resonance parameters (La Cognata et al. 2008a). These were deduced in a simple Breit–Wigner approach, yielding $E_R = 590 \pm 20$ MeV and $\Gamma_{tot} = 208 \pm 26$ MeV (see last line of Table 1), namely a ~10% smaller resonance energy and an intermediate width, as compared with the ones available in the literature. Moreover, an inaccurate estimate of the reaction rate, assuming the narrow resonance approximation, produced a reaction rate larger than the NACRE one.

To understand the origin of such varying experimental widths, the procedures adopted to extract the resonance parameters are briefly reviewed. In Yagi (1962), the *R*-matrix analysis of the excitation function of the $^{18}O + p$ elastic scattering is performed. The resonance energies, spin-parities, and total and partial widths were then extracted for several ^{19}F states in the 8.5–9.5 MeV excitation energy range. From the experimental data, it turns out that the broad 660 keV and 799 keV resonances have the same spin-parity ($J^\pi = 1/2^+$) and display a remarkable interference pattern, making it necessary to adopt a two-level approach in the *R*-matrix application. The resulting 660 keV resonance parameters are given in Table 1. Mak et al. (1978) analyzed the $^{18}O(p,\alpha)^{15}N$ cross section using the *R*-matrix theory. In particular, the authors adopt the same p- and α-channel radii as Yagi (1962), namely 5.1 fm and 5.7 fm, respectively, and perform a simultaneous fit of the scattering and the reaction data. Besides the 660 keV and 799 keV resonances, an additional broad $1/2^-$ level at $E_p = 750$ keV was introduced as a background level, with no physical correspondence, to achieve a satisfactory fit of the cross section, taking care that the extrapolated cross section had a weak dependence on it. A satisfactory fit was obtained for a larger width of the 8.65 MeV ^{19}F level, 160 keV in the laboratory system (Table 1). Lorentz-Wirzba et al. (1979) also performed an *R*-matrix analysis of the $^{18}O(p,\alpha)^{15}N$ cross section, taking into account the constructive (destructive) interference of the 660 keV and 799 keV resonances between (outside) the two levels. The resulting resonance parameters are given in Table 1. A significantly larger width was obtained ($\Gamma_{tot} \sim 324$ keV) in comparison with the previous results.

A better agreement was found among the different authors (Lorentz-Wirzba et al. 1979; Mak et al. 1978; Yagi 1962) about the parameters of the broad resonance near $E_{cm} = 799$ keV (compare Table 2). The only remarkable difference concerns the resonance energy: Christensen et al. (1990) yield $E_R = 789$ keV which is about 10 keV smaller than recommended by the previous works. For these reasons, NACRE adopts the partial widths from Yagi (1962) and Angulo et al. (1999), which are used in the numerical integration to calculate the reaction rate. On the other hand, in the recent review by Iliadis et al. (2010) an average of the existing values was adopted to perform the numerical integration.

The origin of the discrepancy among the resonance parameters for the 660 keV state can be seen clearly if the different experimental data sets for the $^{18}O(p,\alpha)^{15}N$ astrophysical factor $S(E)$ are given in the same figure. Figure 1 shows a linear

Table 2
Level Parameters for 799 keV Resonance

E_R (keV)	Γ_p (keV)	Γ_α (keV)	$\Gamma_{\rm tot}$ (keV)	References
802	25	20	47	Lorentz-Wirzba et al. (1979)
801.5	23.3	18.9	42.2	Mak et al. (1978)
801.5 ± 1.4	24.6 ± 1.4	19.9 ± 0.9	44.5 ± 0.9	Yagi (1962)
789	...	...	...	Christensen et al. (1990)
798.8 ± 1.5	...	...	46 ± 2	Tilley et al. (1995)
798.4 ± 1.6	24.6 ± 1.4	20 ± 1	44.6 ± 1.7	Iliadis et al. (2010)

Notes. Each parameter is given in the center-of-mass system. The parameters from Lorentz-Wirzba et al. (1979) and Mak et al. (1978) are obtained from the *R*-matrix analyses of the measured ^{18}O$(p,\alpha)^{15}$N cross sections. Yagi (1962) extracted the resonance parameters from the *R*-matrix fitting of the ^{18}O + p elastic scattering. Tilley et al. (1995) and Iliadis et al. (2010) are reviews of the existing data.

Table 3
Formal Values of the Proton and Alpha Reduced Width Amplitudes and Resonance Energies for the Indicated Boundary Conditions (BC)

R-Matrix Fitting Parameters	BC	E_1 (MeV)	γ_{p1} (MeV$^{1/2}$)	$\gamma_{\alpha1}$ (MeV$^{1/2}$)	E_2 (MeV)	γ_{p2} (MeV$^{1/2}$)	$\gamma_{\alpha2}$ (MeV$^{1/2}$)
R	$B_c = S_c(E_1)$	0.609	−0.407	0.212	0.845	0.495	0.0706
U	$B_c = S_c(E_1)$	0.607	−0.430	0.215	0.853	0.535	0.0737
L	$B_c = S_c(E_1)$	0.611	−0.387	0.212	0.857	0.590	0.0519
R	$B_c = S_c(E_2)$	0.579	−0.466	0.202	0.813	0.439	0.0967
U	$B_c = S_c(E_2)$	0.572	−0.501	0.202	0.814	0.469	0.103
L	$B_c = S_c(E_2)$	0.582	−0.468	0.202	0.811	0.527	0.0819

Notes. The labels 1 and 2 refer to the 660 keV and 799 keV resonances. The parameters refer to the simultaneous fitting of Lorentz-Wirzba et al. (1979) and THM data (R), of their upper (U), and lower (L) limits. $\tilde{\chi}^2$ is given in the text. The same approach and notation as in Barker (2008) are adopted.

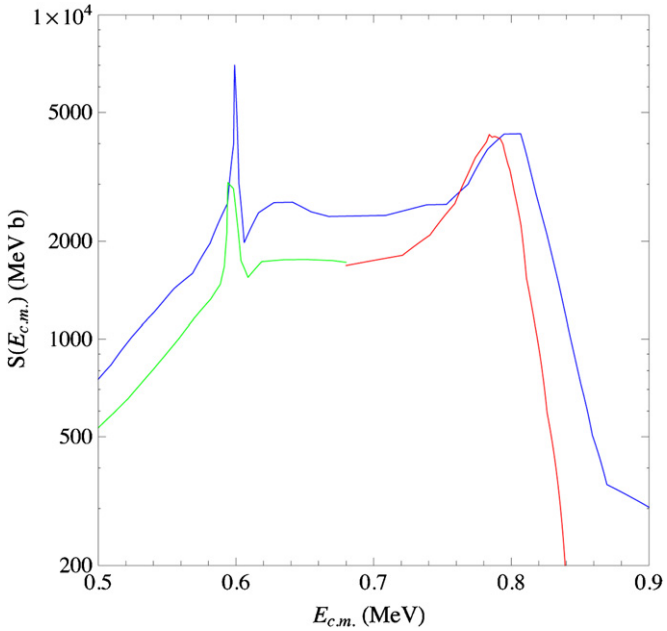

Figure 1. Review of the ^{18}O$(p,\alpha)^{15}$N experimental astrophysical $S(E)$ factor data from Lorentz-Wirzba et al. (1979; blue solid line), Mak et al. (1978; green solid line), and Christensen et al. (1990; red solid line). A remarkable discrepancy shows up between the Lorentz-Wirzba et al. (1979) and Mak et al. (1978) data in the region where the 660 keV broad resonance dominates the cross section.

(A color version of this figure is available in the online journal.)

interpolation of Lorentz-Wirzba et al. (1979) data (blue solid line) together with Mak et al. (1978) data interpolation (green solid line) and the more recent Christensen et al. (1990) data interpolation (red solid line). Apart from the mentioned shift in the 799 keV peak observed by Christensen et al. (1990) in comparison with Lorentz-Wirzba et al. (1979), which may be attributed to a wrong estimate of the target thickness (Christensen et al. 1990), a clear discrepancy is apparent in the absolute value of the experimental $S(E)$ factors around $E_{\rm cm} = 660$ keV. Such a large discrepancy should be attributed to systematic errors of unknown nature, making the deduced reaction rates and the astrophysical predictions based on them potentially flawed. The presence of such untenable discrepancy for this resonance, which spoils the cross section accuracy in the energy region of interest for astrophysics, has motivated the present indirect study via the THM.

This represents the final step in the extensive work on the ^{18}O$(p,\alpha)^{15}$N reaction. The new results concerning the broad high-energy resonances will be merged with the previous ones concerning the narrow low-energy resonances (La Cognata et al. 2008b, 2009a, 2010) to provide an updated reaction rate whose validity range extends over a wide temperature interval for astrophysical modeling.

3. THE THM THEORY: THE MODIFIED *R*-MATRIX APPROACH

The THM was introduced in the early 1990s with the aim of measuring low-energy nuclear reactions severely hindered by the Coulomb barrier for astrophysical application (Baur 1986; Spitaleri 1990; Cherubini et al. 1996; Spitaleri et al. 1999). The THM has been developed in the framework of the plane wave impulse approximation (PWIA; Chew 1950; Jain et al. 1970), which has proved accurate enough to extract the astrophysical $S(E)$ factor (Spitaleri et al. 2004; La Cognata et al. 2010). The analysis of the TH reaction proceeding through a resonance state in the subsystem requires a modified *R*-matrix approach. The reason is that a conventional *R*-matrix method (Lane & Thomas 1958) was developed for analysis of the binary resonant reactions. For a multi-channel, multi-level case, the *R*-matrix

amplitude has quite a complicated form in which the level matrix is expressed in terms of the level energies, level shifts, and reduced widths of the entry and exit channels. The amplitude of the TH reactions, which has three particles in the exit channel instead of the entry-channel reduced widths, contains the binary transfer reaction amplitudes populating resonance states. The question of whether these amplitudes will also appear in the level matrix has been addressed in Mukhamedzhanov et al. (2008) and La Cognata et al. (2010) where, using the shell-model approach to nuclear reactions (Mahaux & Weidenmüller 1969), the generalized R-matrix method has been developed for the two-channel, two-level case. In particular, it was shown that the level-matrix remains the same as in the case of the binary reactions, i.e., it does not contain the transfer reaction amplitudes, which appear only in the nominator instead of the entry channel reduced widths. Here, we provide some details about the THM, focusing on the case of broad resonances.

Let us consider the TH reaction (the two-body to three-body $(2 \to 3)$)

$$a + A \to s + c + C, \tag{1}$$

where $a = (s\,x)$. This TH reaction is used to obtain the astrophysical factor for the binary subreaction

$$x + A \to c + C. \tag{2}$$

We consider the case when the binary subreaction is the resonant one.

The TH reaction amplitude describing the transfer of particle x is given in the post form by (for simplicity, we disregard the spins of the particles)

$$M(P, \mathbf{k}_{aA}) = \left\langle \chi^{(-)}_{\mathbf{k}_{sF}}\, \Phi^{(-)}_F \middle| \Delta V_{sF} \middle| \Psi^{(+)}_i \right\rangle. \tag{3}$$

Here, $\Psi^{(+)}_i$ is the exact $a + A$ scattering wave function; $\Phi^{(-)}_F$ is the wave function of the system $F = c + C = x + A$; $\chi^{(-)}_{\mathbf{k}_{sF}}(\mathbf{r}_{ij})$ is the distorted wave of the system $s + F$; φ_i is the bound state wave function of nucleus i; $\mathbf{r}_{ij}$ and $\mathbf{k}_{ij}$ are the relative coordinate and relative momentum of nuclei i and j; $P = \{\mathbf{k}_{sF}, \mathbf{k}_{cC}\}$ is the six-dimensional momentum describing the three-body system s, c, and C; $\Delta V_{sF} = V_{sF} - U_{sF}$; $V_{sF} = V_{sc} + V_{sC} = V_{sx} + V_{sA}$ is the interaction potential of s and the system F and U_{sF} is their optical potential.

Equation (3), which is the exact expression for the TH reaction amplitude, can be used as a starting point to derive the expression for the TH reaction amplitude proceeding through the interfering resonances in the subsystem F. We neglect the direct coupling between the initial $x + A$ and final $c + C$ channels, which contributes dominantly to direct reactions but gives negligible contribution to resonant ones. An important step in deriving the resonant contribution to the TH reaction matrix element is the spectral decomposition for the wave function $\Phi^{(-)}_F$ given by Equation (3.8.1) of Mahaux & Weidenmüller (1969). It leads to the shell-model-based resonant R-matrix representation for $\Phi^{(-)}_{Fc}$ in channel c, which is similar to the level decomposition for the wave function in the internal region in the R-matrix approach:

$$\Phi^{(-)}_{Fc} \approx \sum_{\nu,\tau=1}^{N} \tilde{V}_{\nu c}(E_c)\, [\mathbf{D}^{-1}]_{\nu\tau}\, \Phi_\tau. \tag{4}$$

Here, N is the number of the levels included, E_c is the relative kinetic energy of nuclei in channel c (in channel $c = c + C$, $E_c \equiv E_{cC}$), and Φ_τ is the bound state wave function describing the compound system F excited to level τ. $\mathbf{D}_{\nu\tau}$ is the same level matrix as in the conventional R-matrix theory and is given by Equation (4.2.20b) of Mahaux & Weidenmüller (1969). It depends on the entry and exit channels reduced width amplitudes, energy levels, and energy shifts. Finally,

$$\tilde{V}_{\nu c}(E_c) = \left\langle \chi^{(-)}_c\, \varphi_c \middle| \Delta V_c \middle| \Phi_\nu \right\rangle \tag{5}$$

is the resonant form factor for the decay of the resonance level ν described by the compound state Φ_ν into channel c, where $\chi^{(-)}_c$ is the distorted wave in channel c. The formal partial resonance width for the decay of this level into channel c is given by

$$\tilde{\Gamma}_{\nu c}(E_c) = 2\,\pi\, |\tilde{V}_{\nu c}(E_c)|^2. \tag{6}$$

In the R-matrix approach, the formal resonance width is related to the formal reduced width $\gamma_{\nu c}$ as $\tilde{\Gamma}_{\nu c}(E_c) = 2\, P_l(E_c, r_{0c})\gamma^2_{\nu c}$, where $P_l(E_c, r_{0c})$ is the barrier penetrability, l is the relative angular orbital momentum of nuclei in channel c, and r_{0c} is the channel radius in channel c. The observable resonance width $\Gamma_{\nu c}$ for the decay of the resonance ν into channel c is related to the formal one by

$$\Gamma_{\nu c} = \frac{\tilde{\Gamma}_{\nu c}\left(E_{R_{\nu c}}\right)}{1 + \sum_{c'} \gamma^2_{\nu c'} \frac{dS_{c'}}{dE_c}\big|_{E_c = E_{R_{\nu c}}}}, \tag{7}$$

provided that boundary condition $B_c = S_c(E_{R_{\nu c}})$, i.e., the energy of the νth level in channel c is $E_{\nu c} = E_{R_{\nu c}}$. Here, $S_c(E_c)$ is the shift factor in channel c, and $E_{R_{\nu c}}$ is the νth resonance energy in channel c. Then, the TH reaction amplitude is

$$M^{(R)}(P, \mathbf{k}_{aA}) \approx \sum_{\nu,\tau=1}^{N} \tilde{V}_{\nu c}(E_c)\, [\mathbf{D}^{-1}]_{\nu\tau} \times M_\tau(\mathbf{k}_{sF}, \mathbf{k}_{aA}), \tag{8}$$

where $M_\tau(\mathbf{k}_{sF}, \mathbf{k}_{aA})$ is the exact amplitude for the direct transfer reaction $a + A \to s + F_\tau$ populating the compound state F_τ of the system $F = x + A = c + C$:

$$M_\tau(\mathbf{k}_{sF}, \mathbf{k}_{aA}) = \left\langle \chi^{(-)}_{sF}\, \Phi_\tau \middle| \Delta V_{sF} \middle| \Psi^{(+)}_i \right\rangle. \tag{9}$$

Equation (8) represents the generalization of the N-level, two-channel R matrix for the TH reaction. As in the conventional R-matrix method, it contains the same level matrix $\mathbf{D}_{\nu\tau}$. In contrast to the conventional R-matrix amplitude for the $x + A \to c + C$ resonant reaction, which contains the entry width amplitude $\tilde{V}_{\tau xA}(E_{xA})$ (Lane & Thomas 1958), the generalized R-matrix amplitude contains the transfer reaction amplitude $M_\tau(\mathbf{k}_{sF}, \mathbf{k}_{aA})$. In practical calculations, the exact $M_\tau(\mathbf{k}_{sF}, \mathbf{k}_{aA})$ can be replaced by the distorted wave Born approximation (DWBA) one:

$$M^{\mathrm{DW}}_\tau(\mathbf{k}_{sF}, \mathbf{k}_{aA}) = \left\langle \chi^{(-)}_{sF}\, \Phi_\tau \middle| \Delta V_{sF} \middle| \varphi_a\, \varphi_A\, \chi^{(+)}_i \right\rangle. \tag{10}$$

The DWBA amplitude takes into account the rescattering of nuclei a and A in the initial state of the TH reaction and enters as a form factor into the TH resonant reaction amplitude. Likewise, for the amplitude of the TH reaction (1) we get from Equation (8) (the exit channel $c = c + C$):

$$M^{(R)}(P, \mathbf{k}_{aA}) \approx \sum_{\nu,\tau=1}^{N} \tilde{V}_{\nu cC}(E_{cC})\, [\mathbf{D}^{-1}]_{\nu\tau} \times M^{\mathrm{DW}}_\tau(\mathbf{k}_{sF}, \mathbf{k}_{aA}). \tag{11}$$

The triple differential cross section for the TH process $a + A \rightarrow s + c + C$ proceeding through interfering resonances is given by Mukhamedzhanov et al. (2008):

$$\frac{d^3\sigma}{dE_{cC}\, d\Omega_{\mathbf{k}_{cC}}\, d\Omega_{\mathbf{k}_{sF}}} = \frac{\mu_{cC}\,\mu_{sF}\,\mu_{aA}}{2\pi^5}\,\frac{k_{cC}\,k_{sF}}{k_{aA}}\,\frac{1}{\hat{J}_a\hat{J}_A} \times \left|\sum_{\nu,\tau=1}^{N} \tilde{V}_{\nu\, cC}(E_{cC})[\mathbf{D}^{-1}]_{\nu\tau} M_\tau(\mathbf{k}_{sF},\mathbf{k}_{aA})\right|^2, \quad (12)$$

where $E_{cC} = k_{cC}^2/(2\,\mu_{cC})$, μ_{ij} is the reduced mass of particles i and j, $\hat{J} = 2J+1$, and J_i is the spin of particle i. For the case of two interfering resonances considered in this paper, $N = 2$. In the THM the half-off-energy-shell (HOES), astrophysical factor is normalized to the on-energy-shell (OES) $S(E_{xA})$ factor for the binary reaction (2), which is given by (for two interfering resonances)

$$S(E_{xA}) = \frac{\mu_{cC}\,\mu_{xA}}{4\pi^2}\,\frac{k_{cC}}{k_{xA}}\,\frac{1}{\hat{J}_x\hat{J}_A}\,E_{xA}\,e^{2\pi\,\eta_{xA}} \times \left|\sum_{\nu,\tau=1}^{2} \tilde{V}_{\nu\, cC}(E_{cC})\,[\mathbf{D}^{-1}]_{\nu\tau}\,\tilde{V}_{\tau\, xA}(E_{xA})\right|^2. \quad (13)$$

Here, η_{xA} is the Coulomb parameter of the x–A nuclei moving with the relative momentum $k_{xA} = \sqrt{2\,\mu_{xA}\,E_{xA}}$. Assume that we normalize the TH astrophysical factor at the second resonance peak. The renormalized TH $S^{\mathrm{TH}}(E_{xA})$ is given by Mukhamedzhanov et al. (2008):

$$S^{\mathrm{TH}}(E_{xA}) = \frac{\mu_{cC}\,\mu_{sF}\,\mu_{aA}}{2\pi^5}\,\frac{k_{cC}\,k_{sF}}{k_{aA}}\,\frac{1}{\hat{J}_a\hat{J}_A}\,E_{xA}\,e^{2\pi\,\eta_{xA}} \times \Gamma_{2\,xA}(E_{xA}) \left|\sum_{\nu,\tau=1}^{2} \tilde{V}_{\nu\, cC}(E_{cC})\,[\mathbf{D}^{-1}]_{\nu\tau} L_{2\,\tau}(\mathbf{k}_{sF},\mathbf{k}_{aA})\right|^2, \quad (14)$$

where

$$L_{2\,\tau}(\mathbf{k}_{sF},\mathbf{k}_{aA}) = \frac{M_\tau(\mathbf{k}_{sF},\mathbf{k}_{aA})}{M_2(\mathbf{k}_{sF},\mathbf{k}_{aA})}, \quad (15)$$

i.e., $L_{22} = 1$ and $L_{21} = M_1/M_2$. Thus, the difference between the TH and OES is the presence in the former of $L_{2\,\tau}(\mathbf{k}_{sF},\mathbf{k}_{aA})$ rather than $\tilde{V}_\tau^{xA}(E_{xA})$. A priori, it can affect the shape of the TH astrophysical factor. However, the matrix $\mathbf{D}^{-1}$ and $\tilde{V}_{\nu\, cC}(E_{cC})$ are the same in the TH and OES astrophysical factors. Hence, fitting to the TH and direct data should provide the same values of the partial and total widths. L_{21} can be used as a complex fitting parameter. If the experimental cross sections for the transfer reactions $a + A \rightarrow s + F_\tau$ populating levels $\tau = 1,\ 2$ at proper energies are available, they can provide $|L_{21}|$ and only the phase of L_{21} will be a fitting parameter.

4. THE EXPERIMENT

The experiment was performed at Laboratori Nazionali del Sud, Catania (Italy). A detailed description can be found in La Cognata et al. (2008b, 2009a, 2010), thus in the following we provide a short discussion of the experimental setup and procedures. The detection setup consisted of a telescope (A), devoted to ^{15}N detection, made up of an ionization chamber and a silicon position sensitive detector (PSD A) on one side with respect to the beam direction. Three additional silicon PSDs (B, C, and D) were placed on the opposite side. Angular conditions were selected in order to maximize the expected quasi free (QF) contribution. To decrease detection thresholds, no ΔE detectors were put in front of PSDs B, C, and D. Energy and position signals of the PSDs were processed by standard electronics together with the time-to-amplitude converter signal for each coincidence event.

The first step of the data analysis was the selection of the ^{2}H(^{18}O,α^{15}N)n reaction channel. Particle identification has been accomplished by means of the ΔE-E technique and by investigating the reaction kinematics. This has allowed us to distinguish the kinematical locus of the ^{2}H(^{18}O,α^{15}N)n reaction from the ones of binary reactions.

As a second step, a thorough study of the reaction dynamics was performed to disentangle the different processes feeding the exit channel. A key test is the study of the neutron momentum distribution. As discussed by La Cognata et al. (2010), good agreement was found between the experimental and theoretical distributions, given by the square of a Hulthèn wave function in momentum space in the PWIA. To check whether the simple PWIA is a viable approach, the DWBA distribution was also evaluated. From the comparison, we found that a good agreement between the two is present for a neutron momentum $p_s < 50$ MeV/c. This demonstrates that the QF mechanism is dominant in such a momentum window (in agreement with the limit set by Shapiro 1967) and that the PWIA provides an accurate framework to extract the resonance parameters for the ^{18}O$(p,\alpha)^{15}$N reaction.

4.1. Extraction of the Cross Section

Angular distributions of the fragments α and ^{15}N, measured from the ^{2}H(^{18}O, α^{15}N)n TH reaction, were then extracted following the PWIA prescription (La Cognata et al. 2010, 2007; Spitaleri et al. 2004).

The resulting THM angular distributions are given in Figure 2 as solid circles. Blue symbols are used for the 145 keV resonance angular distribution, as in La Cognata et al. (2008b, 2010), which has been deduced as a cross check of the data reduction method (La Cognata et al. 2010, 2008b; Spitaleri et al. 2004). Such a distribution is compared with the one measured in direct experiments (Lorentz-Wirzba et al. 1979), given as a straight blue line as the entrance-channel orbital angular momentum is $l = 0$. The THM angular distributions for the two interfering $J^\pi = 1/2^+$ resonances are shown as green and red symbols in Figure 2. From a Gaussian fitting, the resonance energies of these states are about 609 keV and 812 keV, slightly different from what is given in the literature (compare Tables 1 and 2). The THM angular distributions are compared with the direct ones, given as full green and red lines, respectively. These lines are obtained by fitting the experimental data from Lorentz-Wirzba et al. (1979) with first-order cosine polynomials.

Given the good agreement between the experimental THM and direct angular distributions (Figure 2) over the whole range covered here, the angular integration was performed assuming that the trend of the angular distributions is given by the fitted ones (solid lines in Figure 2) outside the range where the THM differential cross section is available. The resulting ^{2}H(^{18}O, α^{15}N)n reaction cross section is shown in Figure 3 (full circles). The error bars account for the statistical uncertainty

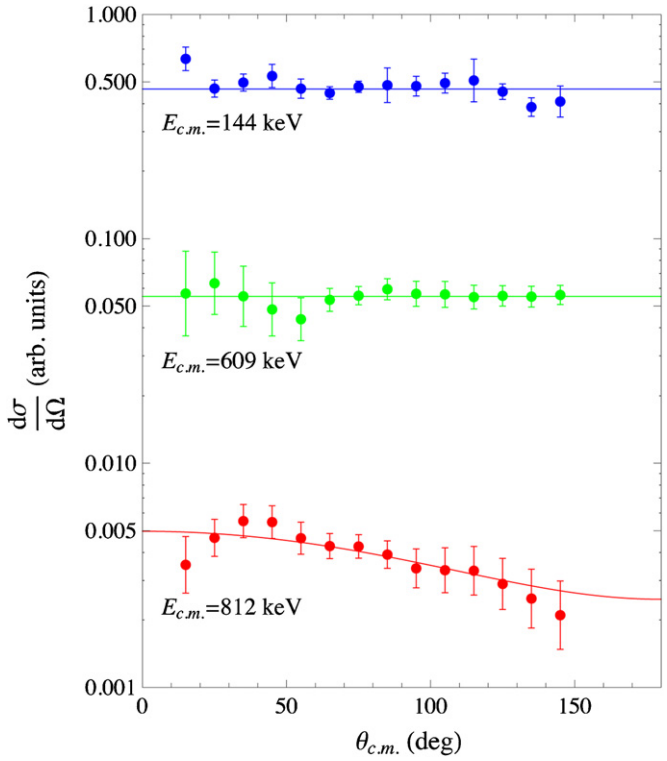

Figure 2. THM angular distributions for the ^{18}O$(p,\alpha)^{15}$N subreaction in the PWIA approach (full dots), compared with the experimental distributions (full lines). These have been obtained by fitting the experimental data from Lorentz-Wirzba et al. (1979) with cosine polynomials. Good agreement is found in the whole angular range for the three energies shown, corresponding to the experimental THM resonance energies.

(A color version of this figure is available in the online journal.)

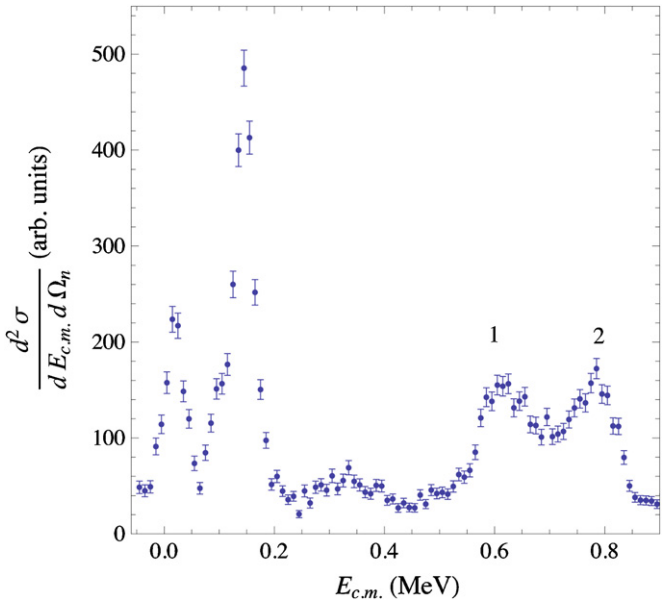

Figure 3. Cross section of the ^{2}H(^{18}O, α^{15}N)n THM reaction, integrated over the whole solid angle using the measured angular distributions inside the range covered by the THM experiment and the trend deduced from Lorentz-Wirzba et al. (1979) outside. Below 200 keV, the same cross section as in La Cognata et al. (2008b, 2009a, 2010) is recovered. Labels 1 and 2 mark the positions of the 660 and 799 keV resonances.

(A color version of this figure is available in the online journal.)

(about 6%, on average) and for the uncertainties coming from the procedure adopted to disentangle the contribution of each resonance to the reaction yield. The 4π integrated cross section in Figure 3 is given in arbitrary units, thus no normalization error is included. Besides the resonances below ~200 keV, the two resonances corresponding to the 8.65 MeV and 8.793 MeV states in ^{19}F are clearly seen. On the other hand, the narrow $3/2^-$ 8.592 MeV ($\Gamma_{\rm tot} = 2$ keV; Tilley et al. 1995), which is clearly observed in direct measurements (compare Angulo et al. 1999; Tilley et al. 1995; Lorentz-Wirzba et al. 1979; Mak et al. 1978 and Figure 1) does not show up. This is understood if the effect of energy resolution is taken into account, namely if direct data are smeared out to match the measured experimental resolution of 17 keV (La Cognata et al. 2008a, 2009b, 2010). Moreover, a bump appears in the $d^2\sigma/dE_{\rm cm}d\Omega_n$ spectrum at about 340 keV, which is not connected to resonances in the ^{18}O$(p,\alpha)^{15}$N cross section. The origin of this contribution can be traced back to sequential decay mechanisms, namely to the decay of unbound states of ^{16}N, as can be deduced from Figure 7 (upper panel) of La Cognata et al. (2010). This enhancement is well separated from the levels of interest, being above $E_{\rm cm} > 500$ keV. In the following, we will focus on this higher energy region to extract the resonance parameters of the 660 keV resonance, thus the effect of such a background state does not affect our conclusions.

The same approach as in La Cognata et al. (2008a, 2010) cannot be used here as broad resonances show up in the cross section, i.e., levels whose E_R is comparable with the total width $\Gamma_{\rm tot}$. In such cases, the modified R-matrix method is suitable. The PWIA is then used to convert the $d^2\sigma/dE_{\rm cm}d\Omega_n$ differential cross section into the astrophysical $S(E)$ factor for the ^{18}O$(p,\alpha)^{15}$N reaction. Indeed, the PWIA provides a very reasonable description of the angular distributions as well as the neutron momentum distribution inside deuteron. It is well known that the PWIA overestimates the absolute value of the differential cross section, but normalization will be performed by scaling the THM $S(E)$ factor to the direct one, which makes the PWIA a good approximation.

5. R-MATRIX SIMULTANEOUS FIT

Direct data in the literature (Lorentz-Wirzba et al. 1979; Mak et al. 1978; Yagi 1962; Christensen et al. 1990) cannot clearly provide a set of coherent resonance parameters to be used in the reaction rate calculations (compare Table 1 and Figure 1). Current compilations (Angulo et al. 1999; Iliadis et al. 2010) have recommended an average of the existing results, which is affected by large errors to account for the discrepancies. Determination of isolated broad resonance parameters is a well-known unsolved problem in physics. The resonance energy and width for a broad resonance are not uniquely defined and many prescriptions have been used in the literature (see Mukhamedzhanov et al. 2010 and references therein). In the case presently under consideration, we have two interfering broad resonances which complicate the problem even more. One of the reasons for simultaneously analyzing the direct data and the TH data is to check which of the existing direct data agree with the TH data. The second reason for the analysis presented in this paper is that we provide the first simultaneous two-channel, two-level R-matrix fit of direct and indirect data.

As discussed in La Cognata et al. (2010), the THM is not sensitive to the entrance channel partial widths but, in this case, the larger uncertainty of the reaction rate is related to the α width of the 660 keV resonance, which has an error of about a

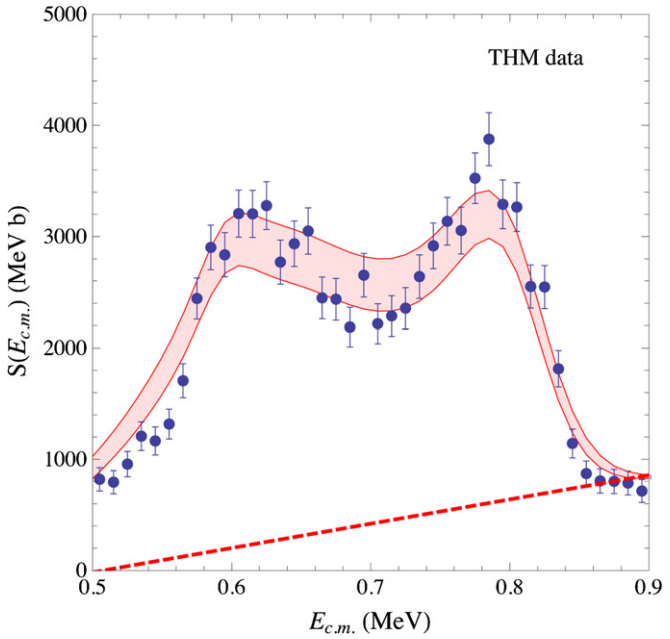

Figure 4. Modified *R*-matrix fitting (red band) of the THM $S(E)$ factor (blue points). The fitting parameters have been determined by simultaneously fitting the Lorentz-Wirzba et al. (1979) and THM data (present work). Moreover, energy resolution has been taken into account by convoluting the fit with the 17 keV energy resolution. The red dashed line shows the background level (see the text for details).

(A color version of this figure is available in the online journal.)

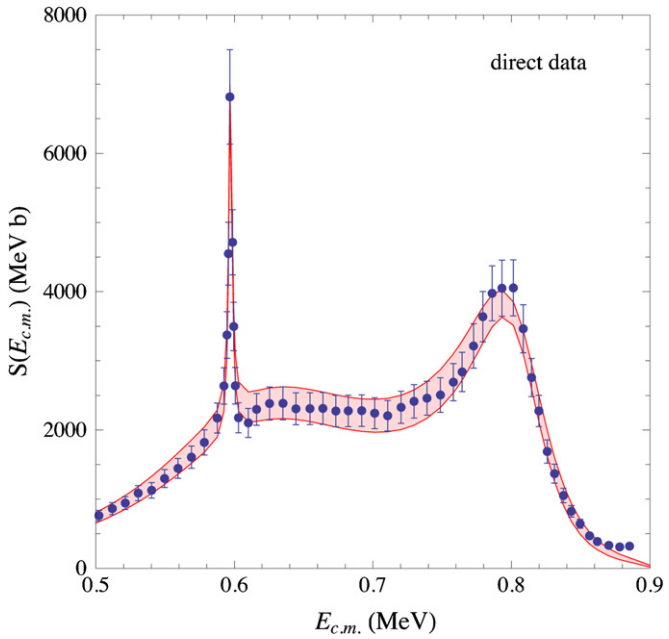

Figure 5. Full two-level, two-channel *R*-matrix fit (red band) of the Lorentz-Wirzba et al. (1979) direct data (blue points). Upper and lower limits of the band are obtained by fitting the upper and lower limits set by the direct data error bars (about 10%). The fitting parameters have been determined by simultaneously fitting the Lorentz-Wirzba et al. (1979) and THM data (present work).

(A color version of this figure is available in the online journal.)

factor of three (compare Table 1). Therefore, the THM is very well suited to indirectly studying the $^{18}O(p,\alpha)^{15}N$ subreaction to reduce the error affecting the Γ_α partial width of the 660 keV resonance.

As a first step, the THM astrophysical $S(E)$ factor has been deduced in the PWIA framework (La Cognata et al. 2007; Spitaleri et al. 2004) in arbitrary units. Normalization is obtained by scaling the THM $S(E)$ factor to fit the direct one from Lorentz-Wirzba et al. (1979), Christensen et al. (1990) possibly having energy calibration problems at the 799 keV resonance. Besides the statistical error, a 3% normalization error has to be added since the fitting is performed over 11 experimental THM points, while the model error, connected with the use of the PWIA, is about 4% (La Cognata et al. 2010). The THM $S(E)$ factor is displayed in Figure 4 as blue dots, where only the statistical error is given. From the comparison of the THM $S(E)$ factor with the $^2H(^{18}O, \alpha^{15}N)n$ QF cross section (Figure 3), it turns out that the difference is very small and within the experimental uncertainties. Regarding the direct data, the astrophysical $S(E)$ factor is taken from Figure 6 (lower panel) of Lorentz-Wirzba et al. (1979). In this figure, errors are barely visible, so they are conservatively estimated to be at least 10% taking into account that the normalization error is 8.8% (since $d\sigma(135^\circ)/d\Omega = 57 \pm 5\ \mu$b/sr; Lorentz-Wirzba et al. 1979). In Figure 5, the Lorentz-Wirzba et al. (1979) $S(E)$ factor is shown as blue symbols.

First, we fit the direct data of Lorentz-Wirzba et al. (1979) in Figure 5 using the genuine two-level, two-channel *R*-matrix approach (Lane & Thomas 1958; La Cognata et al. 2009b). Such an approach is well suited to reproducing the experimental data, in particular the contribution of the 660 keV and 799 keV resonances, since the effect of the interfering 145 keV narrow resonance ($\Gamma_{tot} < 0.3$ keV) can be neglected at such energies (this introduces a systematic error $\leqslant 2\%$ above 0.5 MeV)

Table 4
660 keV and 799 keV Resonance Parameters from the Simultaneous Fitting of Lorentz-Wirzba et al. (1979) and THM data

	E_R (keV)	Γ_p (keV)	Γ_α (keV)	Γ_{tot} (keV)
1	609 ± 2	11.1 ± 1.1	188 ± 3	199 ± 3
2	812.5 ± 1.5	27 ± 10	40^{+5}_{-13}	67^{+11}_{-16}

Notes. The upper and lower limits of the resonance parameters were determined from the two-level, two-channel *R*-matrix fitting of the upper and lower limits of the direct and THM astrophysical $S(E)$ factors. Labels 1 and 2 in the first column refer to the 660 and 790 keV resonances, respectively.

while the 8.629 $7/2^+$ state in ^{19}F adds up incoherently to the $S(E)$ factor. It is worth stressing that neither a non-resonant contribution nor background poles are added, as remarked in Iliadis et al. (2010). The formal and observable fitting parameters are given in Table 3. In the fitting, the interaction radii have been taken as equal to the ones in the literature (Yagi 1962; Mak et al. 1978), namely 5.1 fm for the proton channel and 5.7 fm for the α channel. It is important to explain the procedures for determining the observable resonance energies and widths for overlapping and interfering resonances from the formal parameters. Following Barker (2008) first we select the boundary condition $B_c = S_c(E_1)$ (where $c = p, \alpha$ and S_c is the shift function), so that the first energy level E_1 coincides with the energy of the first resonance (8.65 MeV level in ^{19}F in compilations). After that, we make a fit of the data. From the determined formal values of the proton and alpha reduced width amplitudes of the first resonance, we can determine the observable first resonance energy and observable proton and alpha widths of the first resonance using the standard equations (Lane & Thomas 1958; Barker 2008). After that, we repeat the same procedure fixing the second energy level in the *R*-matrix amplitude at the second resonance energy (8.793 MeV) by taking $B_c = S_c(E_2)$ and, fitting the direct data, we determine

the energy of the second resonance and its observable proton and alpha widths. The determined resonance parameters are given in Table 4. Exactly the same fits may be obtained for any choice of the boundary conditions, provided the values of E_i and γ_{ic} are adjusted suitably. The fitting of Lorentz-Wirzba et al. (1979) has yielded $\tilde{\chi}^2 = 1.8$. It has been performed for the recommended cross sections and for the upper and lower limits set by the experimental uncertainties to determine the resonance parameter associated errors (Table 4). The resulting *R*-matrix fits are given as a light red band in Figure 5, marking the regions allowed for by experimental errors. As we can see from Table 4, the resonance parameters from the two-channel, two-level *R*-matrix fit of the direct data (Lorentz-Wirzba et al. 1979) differ quite significantly from the original fit (compare row 1 of Tables 1 and 2), but no details of the *R*-matrix fitting of Lorentz-Wirzba et al. (1979) are available.

As a second step, we fit the TH $S(E)$ astrophysical factor. Comparing Figures 4 and 5, we see that the shape of the directly measured and TH $S(E)$ factors, in contrast to the narrow resonance case (La Cognata et al. 2010), is quite different for overlapping broad resonances. This is a direct indication that the *R*-matrix amplitudes for analysis of the direct and TH data are different. This difference comes from the presence of the ratio L_{21} in the TH *R*-matrix amplitude rather than the entry to the exit width amplitude in the conventional *R*-matrix approach. To fit the THM $S(E)$ factor, we fix the proton and α formal reduced widths γ_{1p}, $\gamma_{1\alpha}$, γ_{2p}, and $\gamma_{2\alpha}$ for the first and second resonances and the resonance energies E_{R1} and E_{R2} determined from the *R*-matrix fitting of direct data (Lorentz-Wirzba et al. 1979). However, as we have stressed, the modified *R*-matrix amplitude has two additional unknown amplitudes $M_\tau(\mathbf{k}_{sF}, \mathbf{k}_{aA})$, $\tau = 1, 2$, of the direct transfer reactions $^{18}O(d,n)^{19}F_\tau$ populating the first ($\tau = 1$) and second ($\tau = 2$) resonances. Normalization of the TH data to the direct data allows us to express the TH astrophysical factor in terms of the ratio of the direct transfer reaction amplitudes $L_{2\tau}(\mathbf{k}_{sF}, \mathbf{k}_{aA})\mathbf{k}_{sF}, \mathbf{k}_{aA})$, see Equation (14). Using the DWBA, one can check that L_{21} remains practically constant in the significant interval of variation of $\mathbf{k}_{sF}$ near the QF kinematics ($\mathbf{k}_s = m_s/m_a\,\mathbf{k}_a$). That is, we fix L_{21} at the QF kinematics and vary it to fit the TH data by fixing the other parameters at values obtained from the direct data from Lorentz-Wirzba et al. (1979). L_{21} as a complex function can be written as

$$L_{21} = \frac{\gamma_{1p}}{\gamma_{2p}}\, m_{21}\, e^{i\phi_{21}}, \tag{16}$$

i.e., we have two fitting parameters $m_{21} = |L_{21}|$ and its phase factor ϕ_{21}. If the experimental data for transfer reactions $^{18}O(d,n)^{19}F$ populating the 8.65 MeV and 8.793 MeV states of ^{19}F would be available, m_{21} could be determined from the ratio of the experimental differential cross sections. Since these cross sections are not available in the case under consideration, we varied both m_{21} and its phase factor ϕ_{21}. We note that the role of the latter is very important due to a strong interference pattern of two resonances. It is important to remember that THM data have 17 keV energy resolution, which has to be considered when fitting the indirect data. A procedure similar to the one developed in La Cognata et al. (2009b) has been adopted to account for the energy resolution effect, namely the modified *R*-matrix $S(E)$ factor is convoluted with the 17 keV energy resolution estimated in La Cognata et al. (2008b, 2010). The fitting has been performed for the THM $S(E)$ factor (yielding $\tilde{\chi}^2 = 3.0$) and for the upper and lower limits set by the experimental uncertainties. The resulting *R*-matrix fits are given as a light red band in Figure 4, marking the regions allowed for by experimental errors. Regarding the m_{21} and ϕ_{21} parameters, for $B_c = S_c(E_1)$ one gets $m_{21} = 1.09 \pm 0.02$ and $\phi_{21} = -0.32 \pm 0.08$ while for $B_c = S_c(E_1)$ one gets $m_{21} = 1.13 \pm 0.03$ and $\phi_{21} = -0.36 \pm 0.08$. Therefore, the deviation from the OES condition is of the same order as the uncertainty of the experimental data, ~10%, while a significant modification of the interference pattern is retrieved. This is not surprising as a different mechanism for the population of the 660 keV and 799 keV resonances is acting in the THM approach.

To take into account the presence of sequential process events, adding up to the QF yield, in the fit of the THM data a straight line has been added as in La Cognata et al. (2010). The background, as obtained in the fitting, is displayed in Figure 4 as a red dashed line. The dependence of the fitting parameters on the choice of background function has been checked by considering different shapes and varying their relative contribution. It turns out that the change on ϕ_{21} is negligibly small while a maximum change of about 10% affects m_{21}, still within the uncertainty affecting the experimental data.

From Table 4 it turns out that the resonance energy of level 1 is about 50 keV smaller than reported by Yagi (1962), Lorentz-Wirzba et al. (1979), Tilley et al. (1995), and Iliadis et al. (2010) and in good agreement with Mak et al. (1978) and the previous THM measurement (La Cognata et al. 2008a), while a slightly larger E_2 is found—about 10 keV higher than what is listed in the literature (compare the first column of Table 2). Also the proton width for the lower energy resonance Γ_{1p} is larger than the value in the literature, <7 keV, while the α width for the same resonance $\Gamma_{1\alpha}$ is close to the average value estimated by Iliadis et al. (2010), though significantly different from the single estimates except for La Cognata et al. (2008a; column 3 of Table 1). Moving to resonance 2, the resonance parameters from the simultaneous fitting (Table 4) are affected by generally larger errors than those found for the 660 keV resonance because of the large contribution due to such a level that makes it more difficult to estimate Γ_{2p} and $\Gamma_{2\alpha}$. Moreover, Figure 4 demonstrates that in this region the background due to sequential processes is the largest. While Γ_{2p} is in agreement with direct measurement values (column 2 of Table 2), a larger α width is extracted in the present work, even taking into account the experimental uncertainties. As a result, the total width of the 660 keV state $\Gamma_{1\,\mathrm{tot}} = 199 \pm 3$ keV is in good agreement with the mean value adopted by Iliadis et al. (2010) and from the previous THM experiment (La Cognata et al. 2008a), the accuracy being greatly improved. Instead, the total width of the 799 keV resonance turns out to be significantly larger than the values in the literature, about 45 keV. It is worth stressing, anyway, that Yagi (1962) extracted the α width from the proton scattering cross section measurements while Mak et al. (1978) did not cover the region above about 680 keV with their experimental data. This means that their estimates may be affected by systematic errors while the present approach is particularly sensitive on the α widths.

If the same procedure is repeated for the Mak et al. (1978) and Christensen et al. (1990) combined data, to cover the whole 0.5–0.9 MeV range (compare Figure 1), no reasonable simultaneous fitting of direct and THM data have been possible, though the possible shift in energy in Christensen et al. (1990) data was considered in the fitting. This suggests that a consistent picture of the $S(E)$ factor for the $^{18}O(p,\alpha)^{15}N$ reaction in the 0.5–0.9 MeV energy interval can be found only if Mak et al. (1978) data set is not included in the fitting, on the basis of the present THM measurement and the independent one in

La Cognata et al. (2008a). Following this recommendation, the reaction rate has been calculated to evaluate its impact on astrophysics.

6. REACTION RATE

Since the 660 and 799 keV resonances are broad and show an interfering pattern, the narrow resonance approximation cannot be used and numerical integration of the $S(E)$ factor should be performed. To this purpose, the standard equation has been used (Rolfs & Rodney 1988):

$$N_A\langle\sigma v\rangle = \sqrt{\frac{8}{kT}}\frac{1}{(kT)^{3/2}} \times \int_0^\infty S(E)\exp\left(-\frac{E}{kT} - 2\pi\eta\right)dE\,. \quad (17)$$

In the present case, the simultaneous R-matrix fitting of the direct Lorentz-Wirzba et al. (1979) and THM data has been used in the integration, to account for the overlapping contribution of the 660 and 799 keV resonances. The $J^\pi = 1/2^+$ 145 keV resonance also coherently adds up to the 660 keV state, the interference being constructive in the region between the two resonances and destructive outside (Lorentz-Wirzba et al. 1979), while the effect of the tail of the 799 keV resonance is negligible due to the small overlap with the 145 keV level. Therefore, an R-matrix fitting of the Lorentz-Wirzba et al. (1979) data has been performed to take into account the contribution of the 145 keV resonance and of the additional interference effect. Finally, the contributions of the 20 and 90 keV narrow resonances are taken from La Cognata et al. (2010). The resulting total reaction rate is given as a solid thick line in Figure 6, while the contribution of the single resonance is shown as thin lines. In particular, the green line displays the reaction rate component due to the interfering 660 keV and 799 keV resonances, which cannot be considered separately because of the strong interfering pattern. The blue and red lines instead stand for the contribution of the 145 keV and 20 keV resonances, respectively, while the effect of the 90 keV peak is not displayed as it is negligibly small (La Cognata et al. 2010). The validity range of the reaction rate evaluated here extends up to about $T_9 \sim 5$ as the contributions of resonances lying above 0.9 MeV is neglected.

In Table 5 the reaction rate is listed, in cm^3 mol^{-1} s as a function of the temperature T_9. In particular, the recommended, lower, and upper limits are given, the confidence range being fixed by the experimental uncertainties. In the $0.007 < T_9 < 5$ range, the recommended reaction rate has been fitted to provide an analytic expression to be included in astrophysical codes. The resulting equation is

$$\begin{aligned} N_A\langle\sigma v\rangle = {} & \frac{4.76\times10^{11}}{T_9^{2/3}}\exp\left(-\frac{16.74}{T_9^{1/3}} - \left(\frac{T_9}{0.592}\right)^2\right) \\ & \times\left(1 - 2.74\,T_9 + 69.94\,T_9^2\right) \\ & + \frac{1.39\times10^{-13}}{T_9^{3/2}}\exp\left(-\frac{0.232}{T_9}\right) \\ & + \frac{3.34\times10^{4}}{T_9^{3/2}}\exp\left(-\frac{1.685}{T_9}\right) \\ & + \frac{1.903\times10^{9}}{T_9^{1.218}}\exp\left(-\frac{7.528}{T_9}\right), \end{aligned} \quad (18)$$

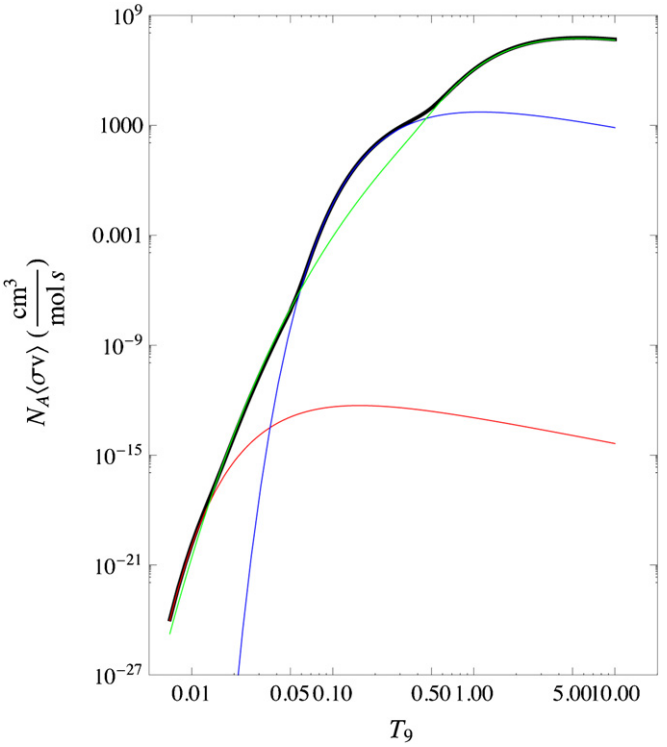

Figure 6. Total rate of the ^{18}O$(p,\alpha)^{15}$N reaction as a function of the temperature T_9 (thick black line), together with the other main contributions to the reaction rate. The thin red line displays the component of the rate due to the 20 keV resonance (La Cognata et al. 2010, 2009a), and the thin blue line shows the contribution of the 145 keV resonance (Lorentz-Wirzba et al. 1979). Finally, the thin green line shows the effect of the combined 660 keV and 799 keV interfering resonances, numerically integrated from the R-matrix simultaneous fitting of Lorentz-Wirzba et al. (1979) and THM data.

(A color version of this figure is available in the online journal.)

yielding $\tilde{\chi}^2 = 1.48$. This expression is obtained by using a formula similar to the NACRE one as a fitting function, leaving the numerical coefficients as free parameters and using the NACRE ones as initialization parameters (Angulo et al. 1999).

A straightforward comparison of our ^{18}O$(p,\alpha)^{15}$N reaction rate with the ones in the most recent compilations (Angulo et al. 1999; Iliadis et al. 2010) is obtained by plotting their ratios. In Figure 7, the ratio to the NACRE rate (Angulo et al. 1999) is given. The light green band represents the range spanned by the NACRE rate, the recommended one being equal to the one in the entire T_9 range. The light red band instead represents the range allowed by the experimental uncertainties of our reaction rate, including the errors of each component contributing to the reaction rate. Clearly, two conclusions can be drawn: (1) there is good agreement between the NACRE compilation rate and the present one below $T_9 = 0.5$ and (2) the reaction rate evaluated here is up to a factor of two larger than the NACRE one above $T_9 = 0.5$. Both considerations can be easily understood by examining Figure 6, since it demonstrates that the 660 keV resonance, whose parameters have been more accurately determined here, is dominant above about $T_9 = 0.5$. Below this temperature, a significant improvement in the rate accuracy has two main causes. (1) The contribution of the 145 keV resonance and the interference effect due to the coherent overlap between the tail of the 660 keV broad resonance and the 145 keV peak are fully taken into account, while in NACRE the upper and lower limits by Mak et al. (1978) are considered, corresponding to constructive and destructive

Table 5
Recommended Values, Lower and Upper Limits of the $^{18}O(p,\alpha)^{15}N$ Reaction Rate as a Function of the Temperature T_9 in cm^3 mol^{-1} s

T_9	Lower	Adopted	Upper
0.007	7.65×10^{-25}	1.07×10^{-24}	1.52×10^{-24}
0.008	3.82×10^{-23}	5.40×10^{-23}	7.68×10^{-23}
0.009	8.15×10^{-22}	1.15×10^{-21}	1.63×10^{-21}
0.010	9.58×10^{-21}	1.34×10^{-20}	1.88×10^{-20}
0.011	7.43×10^{-20}	1.02×10^{-19}	1.42×10^{-19}
0.012	4.32×10^{-19}	5.79×10^{-19}	7.87×10^{-19}
0.013	2.06×10^{-18}	2.68×10^{-18}	3.54×10^{-18}
0.014	8.65×10^{-18}	1.09×10^{-17}	1.38×10^{-17}
0.015	3.31×10^{-17}	4.02×10^{-17}	4.94×10^{-17}
0.016	1.18×10^{-16}	1.39×10^{-16}	1.65×10^{-16}
0.018	1.22×10^{-15}	1.39×10^{-15}	1.58×10^{-15}
0.020	9.76×10^{-15}	1.10×10^{-14}	1.22×10^{-14}
0.025	6.77×10^{-13}	7.53×10^{-13}	8.30×10^{-13}
0.03	1.75×10^{-11}	1.95×10^{-11}	2.14×10^{-11}
0.04	2.06×10^{-9}	2.30×10^{-9}	2.53×10^{-9}
0.05	6.55×10^{-8}	7.30×10^{-8}	8.04×10^{-8}
0.06	2.20×10^{-6}	2.45×10^{-6}	2.70×10^{-6}
0.07	6.35×10^{-5}	7.07×10^{-5}	7.78×10^{-5}
0.08	9.74×10^{-4}	1.08×10^{-3}	1.19×10^{-3}
0.09	8.31×10^{-3}	9.24×10^{-3}	1.02×10^{-2}
0.10	4.59×10^{-2}	5.10×10^{-2}	5.61×10^{-2}
0.11	1.84×10^{-1}	2.05×10^{-1}	2.25×10^{-1}
0.12	5.80×10^{-1}	6.45×10^{-1}	7.09×10^{-1}
0.13	1.52	1.69	1.85
0.14	3.44	3.82	4.20
0.15	6.94	7.71	8.48
0.16	1.27×10^{1}	1.42×10^{1}	1.56×10^{1}
0.18	3.46×10^{1}	3.85×10^{1}	4.23×10^{1}
0.20	7.60×10^{1}	8.44×10^{1}	9.29×10^{1}
0.25	3.01×10^{2}	3.35×10^{2}	3.68×10^{2}
0.30	7.38×10^{2}	8.21×10^{2}	9.03×10^{2}
0.35	1.43×10^{3}	1.59×10^{3}	1.74×10^{3}
0.40	2.52×10^{3}	2.80×10^{3}	3.08×10^{3}
0.45	4.40×10^{3}	4.88×10^{3}	5.37×10^{3}
0.50	7.99×10^{3}	8.88×10^{3}	9.77×10^{3}
0.60	2.89×10^{4}	3.21×10^{4}	3.53×10^{4}
0.70	9.22×10^{4}	1.02×10^{5}	1.13×10^{5}
0.80	2.37×10^{5}	2.63×10^{5}	2.90×10^{5}
0.90	5.26×10^{5}	5.85×10^{5}	6.43×10^{5}
1	1.01×10^{6}	1.12×10^{6}	1.23×10^{6}
1.25	3.24×10^{6}	3.59×10^{6}	3.95×10^{6}
1.5	6.96×10^{6}	7.73×10^{6}	8.51×10^{6}
1.75	1.18×10^{7}	1.31×10^{7}	1.44×10^{7}
2	1.72×10^{7}	1.91×10^{7}	2.10×10^{7}
2.5	2.79×10^{7}	3.10×10^{7}	3.41×10^{7}
3	3.69×10^{7}	4.10×10^{7}	4.51×10^{7}
3.5	4.36×10^{7}	4.85×10^{7}	5.33×10^{7}
4	4.82×10^{7}	5.36×10^{7}	5.89×10^{7}
5	5.27×10^{7}	5.85×10^{7}	6.44×10^{7}

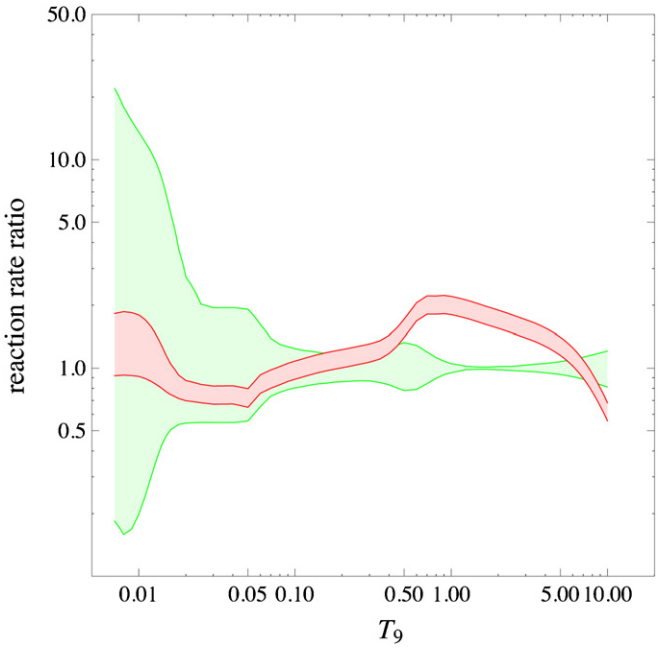

Figure 7. Comparison of the reaction rate calculated here (red band) and the NACRE recommended rate (Angulo et al. 1999; green band). The bands mark the regions allowed by experimental uncertainties. The NACRE recommended rate is presumed equal to 1 over the whole temperature range. A good agreement is found below $T_9 \sim 0.5$ (though the accuracy is largely improved); above $T_9 \sim 0.5$ the 660 keV and the 799 keV dominate and the rate is up to a factor of two larger.

(A color version of this figure is available in the online journal.)

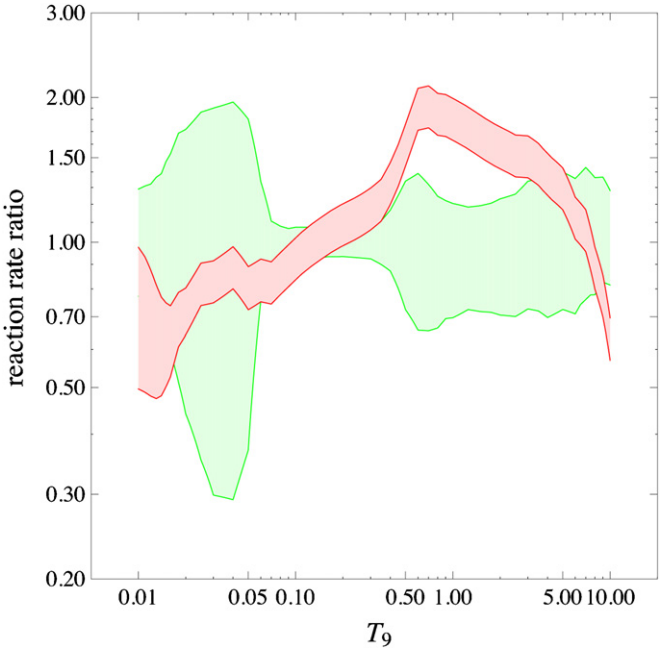

Figure 8. Comparison our reaction rate (red band) and the one given in the recent compilation by Iliadis et al. (2010; green band). Here, the Iliadis et al. (2010) rate is taken as reference, i.e., equal to one the in whole T_9 range, while the bands have the same meaning as in Figure 7. Again, good agreement is found below $T_9 = 0.5$ while at larger temperatures the effect of the new determination of the 660 keV resonance parameters causes a factor of two increase of the reaction rate.

(A color version of this figure is available in the online journal.)

interference, respectively. This is the origin of the difference of Figures 7 and 14 of La Cognata et al. (2010), where the nonresonant rate was taken from NACRE. (2) Below $T_9 = 0.02$, the contribution of the 20 keV resonance is included in the reaction rate calculation (La Cognata et al. 2008b, 2009a, 2010).

Recently, a new reaction rate compilation has been proposed (Iliadis et al. 2010), based on updated nuclear physics input and an improved numerical method for calculating the reaction rate. In Figure 8, the comparison of our reaction rates with those tabulated in Iliadis et al. (2010) is displayed. This is taken as the reference value, namely equal to 1 in the $0.01 < T_9 < 10$ range; the light green band represents the allowed reaction rate range as determined by Iliadis et al. (2010), namely the 0.16 and 0.84 quantiles of the cumulative reaction rate distribution.

As in Figure 7, a light red band provides our allowed range, but taking the ratio to the Iliadis et al. (2010) recommended rate. Again, a good agreement is found between our reaction rate and the Iliadis et al. (2010) reaction rate below $T_9 = 0.5$; it is worth noting that the uncertainty affecting the reaction rate at this low temperature is greatly reduced with respect to NACRE as both the very accurate THM strength of the 20 keV resonance (La Cognata et al. 2010) is included in the calculations and the contribution of the 145 keV resonance as well as the effect of the interference discussed above are taken into account. Moreover, a factor of two discrepancy is still present at higher temperatures since Iliadis et al. (2010) consider an average of the existing 660 keV resonance parameters in the calculations, a procedure similar to the one adopted by NACRE (Angulo et al. 1999), where an average of the numerically integrated reaction rate is recommended.

7. DISCUSSION AND CONCLUSION

A recent THM work (La Cognata et al. 2008a) has suggested that the THM can be employed to solve the problem of the large discrepancy affecting the directly measured $^{18}O(p,\alpha)^{15}N$ cross section in the region around 600 keV and, in particular, the parameters of the broad 660 keV resonance dominating the cross section below 1 MeV. The THM has been used to extract the $S(E)$ factor from the $^2H(^{18}O,\alpha^{15}N)n$ QF reaction performed at 54 MeV beam energy. The resulting $S(E)$ factor has been normalized to the direct data (Lorentz-Wirzba et al. 1979) around 800 keV. Finally, a simultaneous fit of the direct (Lorentz-Wirzba et al. 1979; Mak et al. 1978; Christensen et al. 1990) and THM $S(E)$ factor of the $^{18}O(p,\alpha)^{15}N$ reaction in the 0.5–0.9 MeV energy range has been performed to provide a conclusive set of resonance parameters to be used to calculate the reaction rate. A consistent fitting is obtained by considering the Lorentz-Wirzba et al. (1979) $S(E)$ factor together with the THM one, once the HOES nature of the THM $S(E)$ factor and the 17 keV energy spread have been taken into account. As a consequence, a dramatic improvement of the accuracy of the resonance parameter of the 8.65 MeV ^{19}F state is apparent, the error on its width changing from $\sim$50% to 1.5%, while the resonance energy turns out to be about 50 keV smaller than quoted in the literature (Table 4). This improvement is crucial for astrophysics as the broad 660 keV (and the 799 keV) resonance dominates the reaction rate between $T_9 = 0.5$ and $T_9 = 5$ and strongly influence the low-temperature region through its low-temperature tail (Angulo et al. 1999). As a result, a factor of two increase is found in the reaction rate here determined, due to the recommended resonance parameters, while the rate shows an increased accuracy especially below $T_9 = 0.5$ because the interference between the 145 keV resonance and the tail of the 660 keV peak is fully taken into account in the present calculation (compare Figure 7). A factor of two difference is also found if our reaction rate is compared with the one in Iliadis et al. (2010), where a different and more rigorous technique is used for the reaction rate calculation, but still using an average of the resonance parameters in the literature. Following the considerations discussed in the introduction, the effects of the present results on astrophysics are currently under examination.

This work was supported by the US Department of Energy under grants DE-FG02-93ER40773, DEFG52-06NA26207, and NSF grant PHY-0852653.

REFERENCES

Abia, C., et al. 2009a, PASA, 26, 351
Abia, C., et al. 2009b, ApJ, 694, 971
Abia, C., et al. 2010, ApJ, 715, L94
Angulo, C., et al. 1999, Nucl. Phys. A, 656, 3
Barker, F. C. 2008, Phys. Rev. C, 78, 044611
Baur, G. 1986, Nucl. Phys. A, 458, 188
Busso, M., et al. 2010, ApJ, 717, L47
Champagne, A. E., & Pitt, M. 1986, Nucl. Phys. A, 457, 367
Cherubini, S., et al. 1996, ApJ, 457, 855
Chew, G. F. 1950, Phys. Rev., 80, 196
Christensen, N. S., et al. 1990, Nucl. Instrum. Methods Phys. Res. B, 51, 97
Clayton, G. C., et al. 2007, ApJ, 662, 1220
Coughlan, G. R., & Fowler, W. A. 1988, At. Data Nucl. Data Tables, 40, 283
Iliadis, C., et al. 2010, Nucl. Phys. A, 841, 31
Jain, M., et al. 1970, Nucl. Phys. A, 153, 49
La Cognata, M., et al. 2007, Phys. Rev. C, 76, 065804
La Cognata, M., et al. 2008a, J. Phys. G: Nucl. Part. Phys., 35, 014014
La Cognata, M., et al. 2008b, Phys. Rev. Lett., 101, 152501
La Cognata, M., et al. 2009a, PASA, 26, 237
La Cognata, M., et al. 2009b, Phys. Rev. C, 80, 012801
La Cognata, M., et al. 2010, ApJ, 708, 796
Lane, A. M., & Thomas, R. G. 1958, Rev. Mod. Phys., 30, 257
Lorentz-Wirzba, H., et al. 1979, Nucl. Phys. A, 313, 346
Lugaro, M., et al. 2004, ApJ, 615, 934
Mahaux, C., & Weidenmüller, H. A. 1969, Shell-Model Approach to Nuclear Reactions (Amsterdam: North-Holland)
Mak, H. B., et al. 1978, Nucl. Phys. A, 304, 210
Mukhamedzhanov, A. M., et al. 2008, J. Phys. G: Nucl. Part. Phys., 35, 014016
Mukhamedzhanov, A. M., et al. 2010, Phys. Rev. C, 81, 054314
Nollett, K. M., et al. 2003, ApJ, 582, 1036
Pandey, G., et al. 2008, ApJ, 674, 1068
Rolfs, C., & Rodney, W. S. 1988, Cauldrons in the Cosmos (Chicago, IL: Univ. Chicago Press)
Shapiro, I. S. 1967, in Proc. XXXVIII Int. School of Physics "Enrico Fermi", ed. T. E. O. Ericson (New York: Academic), 210
Spitaleri, C. 1990, in Problems of Fundamental Modern Physics II, ed. R. Cherubini, P. Dalpiaz, & B. Minetti (Singapore: World Scientific), 21
Spitaleri, C., et al. 1999, Phys. Rev. C, 60, 055802
Spitaleri, C., et al. 2004, Phys. Rev. C, 69, 055806
Tilley, D. R., et al. 1995, Nucl. Phys. A, 595, 1
Wiescher, M., & Kettner, K. U. 1982, ApJ, 263, 891
Wiescher, M., et al. 1980, Nucl. Phys. A, 349, 165
Yagi, K. 1962, J. Phys. Soc. Japan, 17, 604
Zinner, E. K. 2005, in Treatise of Geochemistry. I. Meteorites, Comets, and Planets, ed. A. M. Davis (Amsterdam: Elsevier), 17